First-principles calculation of the electron dynamics in crystalline SiO_2

2009 J. Phys.: Condens. Matter 21 064224

(http://iopscience.iop.org/0953-8984/21/6/064224)

IOP Publishing Journal of Physics: Condensed Matter

J. Phys.: Condens. Matter **21** (2009) 064224 (5pp) doi:10.1088/0953-8984/21/6/064224

First-principles calculation of the electron dynamics in crystalline SiO_2

T Otobe[1], K Yabana[2] and J-I Iwata[2]

[1] Advanced Photon Research Center, JAEA, Kizugawa, Kyoto 619-0615, Japan
[2] Center for Computational Sciences, University of Tsukuba, Tsukuba 305-8571, Japan

E-mail: otobe.tomohito@jaea.go.jp

Received 29 June 2008, in final form 1 September 2008
Published 20 January 2009
Online at stacks.iop.org/JPhysCM/21/064224

Abstract

We present a first-principles description for electron dynamics in crystalline SiO_2 induced by an optical field in both weak and intense regimes. We rely upon the time-dependent density-functional theory with the adiabatic local-density approximation, and a real-space and real-time method is employed to solve the time-dependent Kohn–Sham equation. The response calculation to a weak field provides us with information on the dielectric function, while the response to an intense field shows the optical dielectric breakdown. We discuss the critical threshold for the dielectric breakdown of crystalline SiO_2, in comparison with the results for diamond.

(Some figures in this article are in colour only in the electronic version)

1. Introduction

The time-dependent density-functional theory (TDDFT) has been proposed as a tool to describe the quantum dynamics of electrons induced by a time-dependent external potential at the first-principles level [1]. The TDDFT has been most successful in the linear response regime to describe electronic excitations [2, 3]. It has also been applied to nonlinear and nonperturbative dynamics of electrons induced by an intense and ultrashort laser pulse [4].

This paper is intended to present an application of the TDDFT for electron dynamics in bulk crystal of SiO_2, a typical dielectric, induced by an optical field in both weak and intense regimes. This is motivated by the recent experimental progress of laser–materials interaction with intense and ultrashort laser pulses. The key physical process is the optical breakdown creating many electron–hole pairs [5, 6]. This is a highly nonlinear optical process whose mechanism is not yet fully understood [7]. The optical breakdown causes a highly reproducible structure modification on the dielectric, making the process quite suitable for micromachining, medical surgery, and other technical applications [8–10].

There have been several different mechanisms proposed for the origin of the electron–hole pairs which lead to the breakdown. Electron avalanching is considered to be a principal mechanism for pulses longer than a picosecond [5]. For femtosecond pulses, on the other hand, photoionization either by a multiphoton or tunneling mechanism is expected to become dominant. The TDDFT is capable of treating the ionization of both multiphoton [11] and tunneling mechanisms [12]. However, within the adiabatic local-density approximation (ALDA), the electron–electron collisions which cause the electron avalanching are not included. Although all the complex mechanisms are not fully included in the TDDFT with ALDA level, we consider it to be important to clarify to what extent the dielectric breakdown could be quantitatively described within the theory.

We have recently reported the first-principles calculation for the dielectric breakdown of diamond [13]. In that work we clearly demonstrated that the TDDFT is capable of describing the optical dielectric breakdown on a femtosecond timescale. In the present paper we extend our previous work to crystalline α-SiO_2 (α-quarts) for which a number of experimental reports are available [5, 6].

The construction of the present paper is as follows. In section 2 we present a formulation to describe laser–material interaction for a spatially-uniform time-dependent external field. In section 3 we discuss the response for a weak external field which is characterized by the dielectric function. In section 4 we show calculated results of electronic dynamics induced by the intense and ultrashort pulse laser. In section 5 a summary will be presented.

2. Formalism

We here briefly recapitulate our framework to describe the electron dynamics in a crystalline solid. A more complete description will be found in [13, 14]. We consider electron dynamics in an infinite periodic system under a spatially uniform, time-dependent electric field. We thus take a limit of long wavelength and ignore the relation between the frequency and the wavelength of the incident laser pulse. This assumption is valid because the wavelength is much longer than the size of the unit cell. Since we treat the electromagnetic field classically, we ignore the effect of the quantization such as the electron inelastic collision accompanying photoemission. The electron dynamics is described by the following time-dependent Kohn–Sham (TDKS) equation:

$$i\hbar\frac{\partial}{\partial t}\psi_i(\vec{r},t) = H_{\rm KS}(\vec{r},t)\psi_i(\vec{r},t), \tag{1}$$

where $H_{\rm KS}$ is the time-dependent Kohn–Sham Hamiltonian defined by

$$H_{\rm KS}(\vec{r},t) = \frac{1}{2m}\left(\vec{p}+\frac{e}{c}\vec{A}_{\rm tot}(t)\right)^2 + \hat{V}_{\rm ion} + e^2\int d\vec{r}'\,\frac{n(\vec{r},t)}{|\vec{r}-\vec{r}'|} + \hat{\mu}_{\rm xc}(\vec{r},t), \tag{2}$$

e is an elementary charge ($e > 0$), $V_{\rm ion}$ is the electron–ion potential, and $\hat{\mu}_{\rm xc}(\vec{r},t)$ is the exchange–correlation potential. $n(\vec{r},t)$ is the electron density given by $n(\vec{r},t) = \sum_i |\psi_i(\vec{r},t)|^2$. We employ the norm-conserving pseudopotential for $\hat{V}_{\rm ion}$ with the separable approximation [15, 16]. For the exchange–correlation potential, we use that of ALDA with the functional form given in [17].

The time-dependent spatially uniform vector potential $\vec{A}_{\rm tot}(t)$ is composed of the vector potential of an external laser pulse ($\vec{A}_{\rm ext}(t)$) and that of induced polarization ($\vec{A}_{\rm ind}(t)$), $\vec{A}_{\rm tot}(t) = \vec{A}_{\rm ext}(t) + \vec{A}_{\rm ind}(t)$. The induced vector potential satisfies

$$\frac{d^2\vec{A}_{\rm ind}(t)}{dt^2} = \frac{4\pi}{c}\vec{j}(t), \tag{3}$$

where $\vec{j}(t)$ is an electric current density averaged over the unit cell. The macroscopic induced electric field $\vec{F}_{\rm ind}(t)$ is related to the induced vector potential by $\vec{F}_{\rm ind}(t) = -(1/c)(d\vec{A}_{\rm ind}(t)/dt)$. The vector potential of the applied laser pulse is related to the external electric field by $A_{\rm ext}(t) = -c\int F_{\rm ext}(t)\,dt$.

To calculate the electron dynamics in α-SiO_2, we consider a hexagonal unit cell including three SiO_2. To represent the orbital functions $\psi_i(\vec{r},t)$, we introduce a uniform spatial grid in the three-dimensional non-orthogonal coordinates. For 1- and 2-directions, a side of 9.29 au is discretized into 22 grid points, and for the 3-direction, 10.21 au is discretized into 38. As for the Bloch momentum, 8^3 $\vec{k}$-points are employed. We have carefully examined the convergence of the results with respect to these parameters. A high order finite difference approximation is used for the Laplacian, taking 13 points for one direction [19]. The time evolution of the wavefunction for a short period Δt is approximately calculated by the Taylor expansion of the time evolution operator up to fourth order [18]:

$$\psi_i(\vec{r},t+\Delta t) = \sum_{n=1}^{4}\frac{(i\Delta t H_{\rm KS}(\vec{r},t)/\hbar)^n}{n!}\psi_i(\vec{r},t). \tag{4}$$

The time step of $\Delta t = 0.02$ au is used.

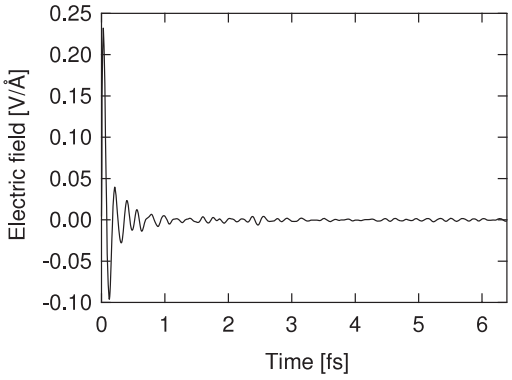

Figure 1. The induced electric field in α-SiO_2 is shown as a function of time after the impulsive electric field is applied at $t = 0$.

3. Linear response calculation

We first consider the response to a weak external field. The responses of infinitely periodic systems to a weak, spatially uniform external field are characterized by the dielectric function $\epsilon(\omega)$. As explained in [14], the dielectric function can be calculated from the real-time evolution of the TDKS equation. For an impulsive external field $A_{\rm ext}(t) = A_0\theta(t)$, we calculate the induced vector potential $A_{\rm ind}(t)$ by solving equations (3). Then the inverse dielectric function is related to the Fourier transform of the induced electric field:

$$\frac{1}{\epsilon(\omega)} - 1 = \frac{1}{A_0}\int_{0+}^{\infty} e^{i\omega t-\gamma t}\frac{dA_{\rm ind}(t)}{dt}\,dt, \tag{5}$$

where γ is a small real number.

We will apply the impulsive electric field to the 3-direction to see the response in that direction. Figure 1 shows the induced electric field as a function of time. The impulsive electric field induces a coherent oscillation of electrons in the crystal. It soon damps in less than 1 fs. This coherent motion corresponds to the plasma oscillation.

We calculate the Fourier transform of the induced electric field to obtain the inverse dielectric function. Figure 2 shows the real and the imaginary parts of the dielectric function. The solid curves show the calculated results and the dashed curves show the measurements [20]. As discussed in [14], the spurious plasmon peak appears at low frequency in the real-time calculation. In order to remove it, we put $\mathrm{Im}\,\epsilon^{-1}(\omega) = 0$ for the frequencies below bandgap and then calculate $\mathrm{Re}\,\epsilon^{-1}(\omega)$ from $\mathrm{Im}\,\epsilon^{-1}(\omega)$ employing the Kramers–Kronig relation. The dielectric function shown in figure 2 is calculated by this procedure.

The calculated value of the static dielectric constant in the 3-direction is 2.67. This is slightly larger than the calculation

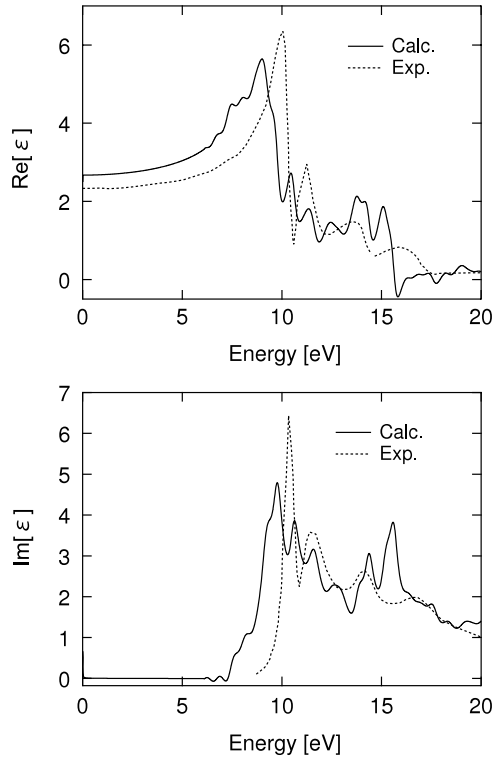

Figure 2. The real part (upper panel) and imaginary part (bottom panel) of the dielectric function of α-SiO_2 are shown. The solid curves show the calculated results employing TDDFT while the dashed curves show the measurement [20].

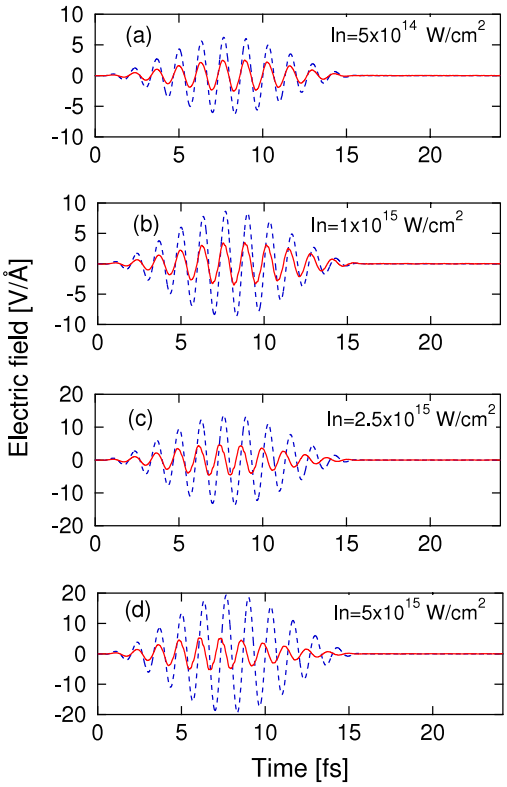

Figure 3. The applied electric field (blue dashed curves) and the total electric field (red solid curves) are shown for laser pulses of different peak intensities: (a) the maximum laser intensity $I = 5 \times 10^{14}$ W cm^{-2}, (b) $I = 1 \times 10^{15}$ W cm^{-2}, (c) $I = 2.5 \times 10^{15}$ W cm^{-2}, and (d) $I = 5 \times 10^{15}$ W cm^{-2}. The laser pulse is applied to α-SiO_2 with the polarization parallel to the z-direction. The laser frequency is set 3.1 eV and the pulse length is 16 fs.

(2.62 in [21]) and the measured value of 2.38 [22]. The dielectric function Re $\epsilon(\omega)$ and Im $\epsilon(\omega)$ looks to shift towards a lower frequency in comparison with the measured value. This may be because of the well-known underestimation of the bandgap energy in the LDA.

The imaginary part Im $\epsilon(\omega)$ shows four sharp and distinct structures at energies of 10.3, 11.7, 14.0, and 17.3 eV. The TDDFT calculation also shows several structures. However, the correspondence is not accurate enough. According to the former studies [23–25], these four peaks correspond to the exciton excitation. The description of the exciton requires treatment of the electron correlation beyond the ALDA. The first-principles description of the excitons in the optical absorption has been achieved by solving the Bethe–Salpeter equation of many-body perturbation theory with the GW approximation [25], density-functional theory (DFT) [23], and TDDFT [24].

4. Response to intense and ultrashort laser pulse

We next discuss the response to intense laser pulses. In figure 3, we show the electric fields of applied laser pulse (blue dotted curves) and the total field inside the crystalline solid (red solid curves) for several laser intensities. The frequency and the pulse length of the laser pulse is chosen to be common, 3.1 eV and 16 fs, respectively. The laser polarization is set parallel to the 3-direction.

At low laser intensity ($I = 5 \times 10^{14}$ W cm^{-2}), the total electric field is almost proportional to the electric field of the applied laser pulse. The ratio between two fields is close to the static dielectric constant, 2.67 in our calculation. Contrary to this case, the phase difference is observed between the applied and the total electric fields at the laser intensity of $I = 1 \times 10^{15}$ W cm^{-2} and higher. The occurrence of the phase difference during the laser irradiation indicates a rapid energy transfer from the laser pulse to the electrons in the crystalline solid and is considered a signature of the breakdown. We observed a similar phase difference in our previous calculations for diamond. In that case, we also observed a plasma oscillation of the excited electrons in the conduction band and it continues even after the applied laser pulse ends. In the present calculation for α-SiO_2, however, we have not observed such an oscillation of the excited electrons after the applied laser pulse ended.

In figure 4, we show the number of excited electrons and the energy transferred from the laser pulse to the electrons as functions of time for a laser pulse of $I = 2.5 \times 10^{15}$ W cm^{-2}. The number of excited electrons (panel (b)) and the energy transfer (panel (c)) clearly show that the appearance of the phase difference between the applied laser pulse and the total electric field is intimately related to the progress of electron excitation.

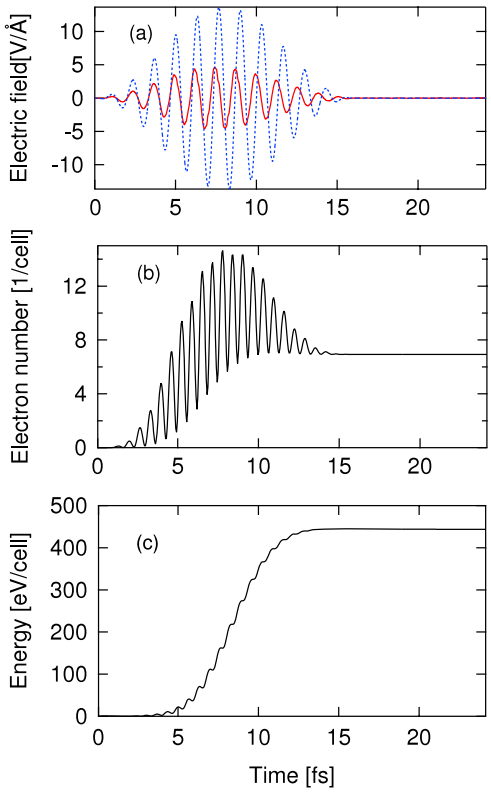

Figure 4. Electron dynamics in α-SiO_2 under the peak intensity of the pulse laser $I = 2.5 \times 10^{15}$ W cm^{-2}, frequency $\hbar\omega = 3.1$ eV, and pulse length 16 fs. The laser polarization is set parallel to the 3-axis. (a) The applied and total electric fields, the same as figure 3(c). (b) The number of electrons excited into conduction band as a function of time. (c) The energy absorbed by the electrons as a function of time.

We may make a simple argument for the occurrence of the breakdown and critical number of excited electrons. Since there is no bandgap for the electrons excited into the conduction band, they can show a plasma oscillation. The plasma frequency ω_p may be estimated by

$$\omega_p = \left(\frac{4\pi n_{ex}}{m\epsilon_0}\right)^{1/2}, \tag{6}$$

where n_{ex} is the number density of excited electrons in the conduction band and ϵ_0 is the static dielectric constant of α-SiO_2. If we evaluate the plasma frequency, putting the number density of excited electrons shown in figure 4(b), we have $\omega_p \simeq 5.62$ eV. This value exceeds the frequency of the applied laser pulse, 3.1 eV. We consider that this fact supports our criterion for judging the occurrence of the optical breakdown from the phase difference between the applied and the total electric fields. Namely, the electrons excited into conduction band start to add a metallic response to the dielectric function. As the number of conduction electrons increases, the plasma frequency also increases. Dielectric breakdown occurs when the plasma frequency reaches the frequency of the applied laser pulse. Then the metallic screening effect dominates in the optical response and a substantial phase difference appears between the applied and total electric fields.

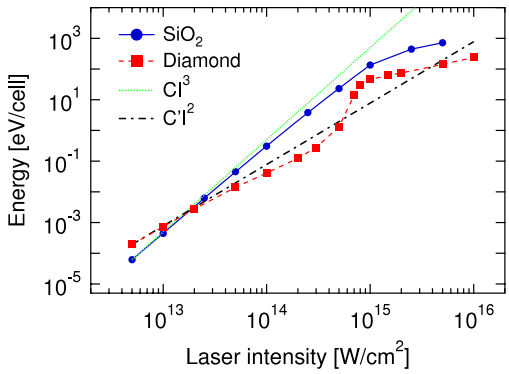

Figure 5. The energy absorbed by the electrons is plotted as a function of the peak laser intensity. The frequency and the pulse length of the laser pulse is fixed at 3.1 eV and 16 fs, respectively. The blue solid curve with filled circles shows the results for SiO_2 while the red dashed curve with filled squares shows the results for diamond [13]. The green dotted line is $\delta E \propto CI^3$, which implies three-photon absorption, and black dot–dashed line is $\delta E \propto C'I^2$, which implies two-photon absorption. These two lines are normalized so that they coincide with the value of a real-time calculation at $I = 5 \times 10^{12}$ W cm^{-2}.

Finally, we show the energy transferred from the laser pulse to the electrons in a crystalline solid in figure 5. The blue solid curve with circles indicates the present calculation, while the red dashed curve with squares indicates our previous calculation for diamond. In two calculations of the present α-SiO_2 and the previous diamond, we employ the laser pulse of the same time profile. The straight dotted lines indicate the three-photon absorption for α-SiO_2 and the black dot–dashed line indicates the two-photon absorption for diamond. Since the bandgap for diamond in LDA is 4.8 eV, two photons are required to excite the electrons across the bandgap. The direct bandgap of α-SiO_2 is 6.1 eV in our calculation. This means that two-photon absorption could promote the excitation across the bandgap. However, a good fit of the $\propto I^3$ line for the calculated result in the low intensity region indicates that the energy transfer from the laser pulse to the electrons proceeds dominantly through three-photon absorption. The strength of the electric field at the breakdown threshold, 1×10^{15} W cm^{-2}, roughly coincides with that in the material which binds valence electrons to ions. We note that, at this laser intensity, the nonlinear ionization mechanism such as the tunnel ionization become substantial in atoms and molecules under intense laser pulses.

In the case of diamond, an abrupt increase of the energy transfer is observed at a laser strength of 7×10^{14} W cm^{-2}. We confirmed that this strength coincides with the occurrence of the phase difference between the applied and the total electric field. For α-SiO_2, on the other hand, the energy transfer shows a gradual decrease from the three-photon line and no peculiar behavior is observed at the occurrence of the optical breakdown. Further investigations are needed to understand the different behaviors in α-SiO_2 and diamond.

5. Summary

We have reported the first-principles calculations for optical responses of α-SiO_2 within the TDDFT with the real-time and

real-space method. We first show the real-time calculation of the dielectric function. Although exciton structures cannot be described adequately within the ALDA, a reasonable description is observed for an overall behavior of the dielectric function. We then show the response to an intense and ultrashort laser pulse. We have found that the phase difference starts to appear at a laser intensity of $I = 2.5 \times 10^{15}$ W cm^{-2} between the applied laser pulse and the total electric field. We regard the phase difference as a signature of dielectric breakdown. Comparing the present result with our previous calculation, the critical laser intensity for the breakdown of α-SiO_2 is about a factor of three higher than that for diamond.

Acknowledgments

This work is supported by Grants-in-Aid for Scientific Research (nos 19019002, 18540366, and 17540231). Numerical calculations were achieved on the supercomputer Altix3700Bx2 at the Japan Atomic Energy Agency (JAEA) and the parallel computer at the Advanced Photon Research Center (APRC).

References

[1] Runge E and Gross E K U 1984 *Phys. Rev. Lett.* **52** 997
[2] Yabana K and Bertsch G F 1999 *Int. J. Quantum Chem.* **75** 55
[3] Yabana K, Nakatsukasa T, Iwata J-I and Bertsch G F 2006 *Phys. Status Solidi* b **243** 1121
[4] Petersilka M and Gross E K U 1999 *Laser Phys.* **9** 105
[5] Mao S S *et al* 2004 *Appl. Phys.* A **79** 1695
[6] Winkler S W *et al* 2006 *Appl. Phys.* A **84** 413
[7] Rethfeld B 2004 *Phys. Rev. Lett.* **92** 187401
Rethfeld B 2006 *Phys. Rev. Lett.* B **73** 035101
[8] Shimotsuma Y, Kazansky P G, Qiu J and Hirao K 2003 *Phys. Rev. Lett.* **91** 247405
[9] Vogel A, Noack J, Huttman G and Paltauf G 2005 *Appl. Phys.* B **81** 1015
[10] Bhardwaj V R *et al* 2006 *Phys. Rev. Lett.* **96** 057404
[11] Gross E K U *et al* 1996 *Top. Curr. Chem.* **181** 81
[12] Otobe T, Yabana K and Iwata J-I 2004 *Phys. Rev.* A **69** 053404
[13] Otobe T, Yamagiwa M, Iwata J-I, Yabana K, Nakatsukasa T and Bertsch G F 2008 *Phys. Rev.* B **77** 165104
[14] Bertsch G F, Iwata J-I, Rubio A and Yabana K 2000 *Phys. Rev.* B **62** 7998
[15] Troullier N and Martins J L 1991 *Phys. Rev.* B **43** 1993
[16] Kleinman L and Bylander D M 1982 *Phys. Rev.* B **48** 1425
[17] Perdew J P and Zunger A 1981 *Phys. Rev.* B **23** 5048
[18] Yabana K and Bertsch G F 1996 *Phys. Rev.* B **54** 4484
[19] Chelikowsky J, Troullier N, Wu K and Saad Y 1994 *Phys. Rev.* B **50** 11355
[20] Philipp H R 1966 *Solid State Commun.* **4** 73
[21] Donadio D, Bernasconi M and Tassone F 2003 *Phys. Rev.* B **68** 134202
[22] Gervais F and Piriou B 1975 *Phys. Rev.* B **11** 3944
[23] Xu Y-N and Ching W Y 1991 *Phys. Rev.* B **44** 11048
[24] Marini A, Del Sole R and Rubio A 2003 *Phys. Rev. Lett.* **91** 256402
[25] Chang E K, Rohlfing M and Louie S G 2000 *Phys. Rev. Lett.* **85** 2613